

# On the effect of surfactant adsorption and viscosity change on apparent slip in hydrophobic microchannels

Christian Kunert and Jens Harting

Institute for Computational Physics,  
University of Stuttgart, Pfaffenwaldring 27, D-70569 Stuttgart, Germany

**Abstract:** Substantial experimental, theoretical, as well as numerical effort has been invested to understand the effect of boundary slippage in microfluidic devices. However, even though such devices are becoming increasingly important in scientific, medical, and industrial applications, a satisfactory understanding of the phenomenon is still lacking. This is due to the extremely precise experiments needed to study the problem and the large number of tunable parameters in such systems.

In this paper we apply a recently introduced algorithm to implement hydrophobic fluid-wall interactions in the lattice Boltzmann method. We find a possible explanation for some experiments observing a slip length depending on the flow velocity which is contradictory to many theoretical results and simulations. Our explanation is that a velocity dependent slip can be detected if the flow profile is not fully developed within the channel, but in a transient state.

Further, we show a decrease of the measured slip length with increasing viscosity and demonstrate the effect of adding surfactant to a fluid flow in a hydrophobic microchannel. The addition of surfactant can shield the repulsive potential of hydrophobic walls, thus lowering the amount of slip with increasing surfactant concentration.

**Keywords:** lattice Boltzmann, microflows, apparent slip

---

## Introduction

---

Microflow devices are used for chemical, biological, or medical analysis techniques. Putting the “lab on a chip” allows to minimize the time needed for the analysis with only small amounts of fluid. Also, such microdevices are more mobile and allow a parallel treatment of multiple fluids. Other microflow systems are used as sensors and actuators for devices like chemical reactors, cars, airplanes and inkjet printers.

In these miniature apparatuses, a number of effects appear which cannot easily be explained with our conventional physical understanding. A common example is the violation of the no-slip boundary condition. The no-slip boundary condition is one of the fundamental assumptions common in classical fluid mechanics, stating that the velocity of a fluid at a wall is equal to the velocity of the wall. For macroscopic applications no-slip is undoubted but during recent years a number of experiments found a violation of the no-slip boundary condition on a length scale of nanometers up to micrometers (1; 2). Numerous experiments (1; 2; 3; 4; 5; 6; 7; 8; 9) utilize a modified atomic force microscope (AFM) with an oscillating col-

loidal sphere at the tip of its cantilever to measure the force needed to displace the fluid between the colloidal sphere and a wall. From the detected force, the amount of wall-slippage can be estimated as described in (3). Other authors like Tretheway and Meinhart apply particle image velocimetry (PIV) to observe the flow near the fluid-wall boundary directly to quantify wall slippage (10; 11). However, it is still an open question if the detected slip is a fundamental property or appears due to surface variations, uncertainties in the experimental setups, or the complex interactions between fluid and wall.

Instead of the no-slip boundary condition, Navier introduced in 1823 a slip boundary condition where the transversal velocity near the wall  $v_z(x=0)$  is proportional to the shear rate  $\frac{\partial v_z}{\partial x}$  and the so called slip length  $\beta$  (12),

$$v_z(x=0) = \beta \frac{\partial v_z}{\partial x} \Big|_{x=0}. \quad (1)$$

Here, the boundary is at  $x=0$ .  $z$  is the flow direction and  $v_z$  is the fluid velocity in flow direction, parallel to the wall. The slip length  $\beta$  can be interpreted as the distance between the wall and the virtual point inside the wall at which the extrapolated flow velocity would be zero.

Due to the large number of tunable experimental parameters like temperature, viscosity, flow velocity, pressure, or surface properties, as well as their individual dependencies on each other, it is not possible to cover all occurring phenomena in a single experiment. In fact, a change in the surface properties usually implies a different experimental setup and a change of viscosity without varying the temperature is only possible by a replacement of the fluid. However, such strong interventions might also have an influence on other parameters of the system. In computer simulations it is possible to vary a single parameter of the fluid, e.g., the viscosity or the density, without changing other parameters. This is important to improve our understanding of the effects occurring in microfluidic systems and to further promote the design of such devices.

In addition, computer simulations are able to study the properties of multiphase flows in microchannels with the individual fluid parameters and fluid-fluid interactions being well defined. In particular, the influence of surfactant is of interest here. Surfactant molecules are often called amphiphiles and are comprised of a hydrophilic (water-loving) head group and a hydrophobic (oil-loving) tail. In a non-wetting microchannel filled with water, the surfactant molecules arrange at the interface between water and surface, thus shielding the hydrophobic repulsion of the wall. On the other hand, in a wetting channel an arrangement of surfactant molecules at the boundary causes the otherwise wetting wall to become hydrophobic. As a result an apparent slip occurs.

---

## 2 Simulation method

---

The simulation method used to study microfluidic devices has to be chosen carefully. While Navier-Stokes solvers are able to cover most problems in fluid dynamics, they lack the possibility to include the influence of molecular interactions as needed to model boundary slip. Molecular dynamics simulations (MD) are the best choice to simulate the fluid-wall interaction, but the computer power today is not sufficient to simulate length and time scales necessary to achieve orders of magnitude which are relevant for experiments. However, boundary slip with a slip length  $\beta$  of the order of many molecular diameters  $\sigma$  has been studied with molecular dynamics simulations by various authors (13; 14; 15; 16; 17; 18; 19). They find increasing slip with decreasing liquid density and liquid-solid interactions as well as a decrease of slip with increasing pressure. However, the maximum number of particles that can be simulated on today's most powerful supercomputers is about 20 billion (20). This corresponds to a volume of less than one  $\mu\text{m}^3$ , but the typical length scale of a microfluidic device is about  $100\mu\text{m}$ .

A mesoscopic model is able to govern a volume large enough to describe the flow properties and still holds information about the molecular behavior. The term “mesoscopic” means that the trajectories of single molecules are not simulated in detail but a whole ensemble of “quasi

particles” behaves as the corresponding real microscopic system. Due to this coarse-graining, the numerical effort is much smaller than for molecular dynamics simulations because the collision and propagation rules of the used “quasi particles” are much simpler than the ones of real particles. Therefore, much larger particle counts can be simulated for substantially longer times. An example for a mesoscopic simulation method is “stochastic rotation dynamics” (SRD), which is sometimes called “multi particle collision dynamics” (MPCD). In a propagation step, every representative fluid particle is moved according to its velocity to its new position. In the collision step, the simulation volume is split into boxes. In each box the velocity vectors of every single particle are rotated around the mean velocity in a random manner, so that energy and momentum are conserved in every box (21; 22). The method is efficient and is used when Brownian motion is required. Its disadvantage is that thermal fluctuations cannot be switched off. “Dissipative particle dynamics” (DPD) also utilizes quasi particles which represent a set of molecules. The propagation of such a collective quasi particle is implemented as in molecular dynamics but collisions are dissipative. This method is easy to implement in an existing MD simulation code but the computational costs are still very high.

In this paper we use the lattice Boltzmann method, where one discretizes the Boltzmann kinetic equation

$$\left[ \frac{\partial}{\partial t} + v \nabla_x + \frac{1}{m} \mathbf{F} \nabla_v \right] \eta(\mathbf{x}, \mathbf{v}, t) = \Omega \quad (2)$$

on a lattice.  $\eta$  indicates the probability to find a single particle with mass  $m$ , velocity  $\mathbf{v}$  at the time  $t$  at position  $\mathbf{x}$ . The derivatives represent simple propagation of a single particle in real and velocity space whereas the collision operator  $\Omega$  takes into account molecular collisions in which a particle changes its momentum due to a collision with another particle. External forces  $\mathbf{F}$  can be employed to implement the effect of gravity or external fields. To represent the correct physics, the collision operator should conserve mass, momentum, and energy, and should be Galilei invariant. By performing a Chapman Enskog procedure, it can be shown that such a collision operator  $\Omega$  reproduces the Navier-Stokes equation (23). In the lattice Boltzmann method the time  $t$ , the position  $\mathbf{x}$ , and the velocity  $\mathbf{v}$  are discretized.

During the last years a number of attempts to simulate slip within the lattice Boltzmann method have been developed. The most simple idea is to use a partial bounce back boundary condition (23). While full bounce back leads to no slip, full reflection leads to full slip. Partial slip implies that a particle is reflected by the wall with the probability  $q$ , while it bounces back with probability  $(1 - q)$ . As a result, a finite boundary slip can be observed. Nie et al. (24) use a Knudsen-number dependent relaxation time in the vicinity of the wall to generate slippage in an ideal gas lattice Boltzmann model.

Our attempt to generate slip involves a repulsive potential at the wall (25). This leads to a depletion zone

near the wall with a reduced density resulting in an apparent slip at hydrophobic (non wetting) walls. Benzi et al. (26) introduced a similar approach but the repulsion there decays exponentially while the potential we are using only takes into account next neighbor lattice sites as described below. Our method is based on Shan and Chen's multiphase lattice Boltzmann method, i.e., the interaction between the surface and the fluid is simulated similar to the interactions between two fluid phases. This allows us to recycle our well tested parallel 3D multiphase lattice Boltzmann code, as it is presented in (27) with only minor modifications. It is very advantageous of our model that its parameters can be linked to experimentally available properties, namely the contact angle (28).

The simulation method and our implementation of boundary conditions are described as follows. A multiphase lattice Boltzmann system can be represented by a set of equations (29)

$$\eta_i^\alpha(\mathbf{x} + \mathbf{c}_i, t + 1) - \eta_i^\alpha(\mathbf{x}, t) = \Omega_i^\alpha, \quad i = 0, 1, \dots, b, \quad (3)$$

where  $\eta_i^\alpha(\mathbf{x}, t)$  is the single-particle distribution function, indicating the amount of species  $\alpha$  with velocity  $\mathbf{c}_i$ , at site  $\mathbf{x}$  on a D-dimensional lattice of coordination number  $b$  (D3Q19 in our implementation), at time-step  $t$ . This is a discretized version of equation (2) without external forces  $\mathbf{F}$  for a number of species  $\alpha$ . For the collision operator  $\Omega_i^\alpha$  we choose the Bhatnagar-Gross-Krook (BGK) form (30)

$$\Omega_i^\alpha = -\frac{1}{\tau^\alpha}(\eta_i^\alpha(\mathbf{x}, t) - \eta_i^{\alpha eq}(\mathbf{u}^\alpha(\mathbf{x}, t), \eta^\alpha(\mathbf{x}, t))), \quad (4)$$

where  $\tau^\alpha$  is the mean collision time for component  $\alpha$  and determines the kinematic viscosity

$$\nu^\alpha = \frac{2\tau^\alpha - 1}{6}. \quad (5)$$

of the fluid. The system relaxes to an equilibrium distribution  $\eta_i^{\alpha eq}$  which can be derived imposing restrictions on the microscopic processes, such as explicit mass and momentum conservation for each species (31; 32; 33). In our implementation we choose for the equilibrium distribution function

$$\eta_i^{\alpha eq} = \zeta_i \eta^\alpha \left[ 1 + \frac{\mathbf{c}_i \cdot \mathbf{u}}{c_s^2} + \frac{(\mathbf{c}_i \cdot \mathbf{u})^2}{2c_s^4} - \frac{u^2}{2c_s^2} + \frac{(\mathbf{c}_i \cdot \mathbf{u})^3}{6c_s^6} - \frac{u^2(\mathbf{c}_i \cdot \mathbf{u})}{2c_s^4} \right], \quad (6)$$

which is a polynomial expansion of the Maxwell distribution.  $\mathbf{c}_i$  are the velocity vectors pointing to neighbouring lattice sites.  $c_s = 1/\sqrt{3}$  is the speed of sound for the D3Q19 lattice. The macroscopic values can be derived from the single-particle distribution function  $\eta_i^\alpha(\vec{x}, t)$ , i.e., the density  $\eta^\alpha(\vec{x})$  of the species  $\alpha$  at lattice site  $\vec{x}$  is the sum over the distribution functions  $\eta_i^\alpha(\vec{x})$  for all lattice velocities  $\vec{c}_i$

$$\eta^\alpha(\mathbf{x}, t) \equiv \sum_i \eta_i^\alpha(\mathbf{x}, t). \quad (7)$$

$\mathbf{u}^\alpha(\mathbf{x}, t)$  is the macroscopic velocity of the fluid, defined as

$$\eta^\alpha(\mathbf{x}, t) \mathbf{u}^\alpha(\mathbf{x}, t) \equiv \sum_i \eta_i^\alpha(\mathbf{x}, t) \mathbf{c}_i. \quad (8)$$

Interactions between different fluid species are introduced following Shan and Chen as a mean field body force between nearest neighbors (34; 35),

$$\mathbf{F}^\alpha(\mathbf{x}, t) \equiv -\psi^\alpha(\mathbf{x}, t) \sum_{\bar{\alpha}} g_{\alpha\bar{\alpha}} \sum_{\mathbf{x}'} \psi^{\bar{\alpha}}(\mathbf{x}', t) (\mathbf{x}' - \mathbf{x}), \quad (9)$$

where  $\psi^\alpha(\mathbf{x}, t) = (1 - e^{-\eta^\alpha(\mathbf{x}, t)/\eta_0})$  is the so-called effective mass with  $\eta_0$  being a reference density that is set to 1 in our case (34).  $g_{\alpha\bar{\alpha}}$  is a force coupling constant, whose magnitude controls the strength of the interaction between component  $\alpha$  and  $\bar{\alpha}$ . The dynamical effect of the force is realized in the BGK collision operator (4) by adding an increment  $\delta \mathbf{u}^\alpha = \tau^\alpha \mathbf{F}^\alpha / \eta^\alpha$  to the velocity  $\mathbf{u}$  in the equilibrium distribution function (6). For the potential of the wall we attach the imaginary fluid “density”  $\eta^{\text{wall}}$  to the first lattice site inside the wall. The only difference between  $\eta^{\text{wall}}$  and any other fluid packages on the lattice  $\eta^{\bar{\alpha}}$  is that the fluid corresponding to  $\eta^{\text{wall}}$  is only taken into account for in the collision step, but not in the propagation step. Therefore, we can adopt  $\eta^{\text{wall}}$  and the coupling constant  $g_{\alpha, \text{wall}}$  in order to tune the fluid-wall interaction.  $g_{\alpha, \text{wall}}$  is kept at 0.08 throughout this paper if not mentioned otherwise and all values are reported in lattice units. Additionally, we apply second order correct mid-grid bounce back boundary conditions between the fluid and the surface (23).

Amphiphiles are introduced within the model as described in (36) and (37). An amphiphile usually possesses two different fragments, one being hydrophobic and one being hydrophilic. The orientation of any amphiphile present at a lattice site  $\mathbf{x}$  is represented by an average dipole vector  $\mathbf{d}(\mathbf{x}, t)$ . Its direction is allowed to vary continuously and to keep the model as simple as possible no information is specified for velocities  $\mathbf{c}_i$ . The surfactant density at a given site is given by an additional fluid species with density  $\eta^{\text{sur}}$ , that behaves as every other species  $\alpha$ . The direction  $\mathbf{d}(\mathbf{x}, t)$  propagates with the fluid field according to

$$\eta^{\text{sur}}(\mathbf{x}, t+1) \mathbf{d}(\mathbf{x}, t+1) = \sum_i \eta_i^{\text{sur}}(\mathbf{x} - \mathbf{c}_i, t) \mathbf{d}'(\mathbf{x} - \mathbf{c}_i, t) \quad (10)$$

and during the collision step the direction  $\mathbf{d}$  evolves to the equilibrium direction  $\mathbf{d}^{\text{eq}}$  similar to the BGK operator

$$\mathbf{d}'(\mathbf{x}, t) = \mathbf{d}(\mathbf{x}, t) - \frac{\mathbf{d}(\mathbf{x}, t) - \mathbf{d}^{\text{eq}}(\mathbf{x}, t)}{\tau^d} \quad (11)$$

( $\mathbf{d}'$  indicates the direction after the collision step). The equilibrium distribution  $\mathbf{d}^{\text{eq}} \simeq \frac{d_0}{3} \mathbf{h}$  is proportional to the so called color field or order parameter  $h$  which represents the distribution of the other species. It is defined as the weighted sum of the densities of all species

$$h(\mathbf{x}, t) = \sum_\alpha \epsilon^\alpha \eta^\alpha(\mathbf{x}, t). \quad (12)$$

In our case ( $\alpha = 2$ ) we set the weights to  $\epsilon^\alpha = \pm 1$ , i.e.,  $h$  corresponds to the density difference between the two species.

The model has been used successfully to study spinodal decomposition (38; 39), binary and ternary amphiphilic fluids under shear (40), the formation of mesophases (41; 42; 43; 44; 45; 46), and flow in porous media (47). Of particular relevance for the present paper is our first article on simulations of apparent slip in hydrophobic microchannels (25).

### 3 Simulation setup

The simulations in this work use a setup of two infinite planes separated by the distance  $2d$ . We call the direction between the two planes  $x$  and if not stated otherwise  $2d$  is set to 64 lattice sites. In  $y$  direction we apply periodic boundary conditions. Here, 8 lattice sites are sufficient to avoid finite size effects, since there is no propagation in this direction.  $z$  is the direction of the flow with our channels being 512 lattice sites long. At the beginning of the simulation ( $t = 0$ ) the fluid is at rest. We then apply a pressure gradient  $\nabla p$  in the  $z$ -direction to generate a planar Poiseuille flow. Assuming Navier's boundary condition (1), the slip length  $\beta$  is measured by fitting the theoretical velocity profile,

$$v_z(x) = \frac{1}{2\mu} \frac{\partial P}{\partial z} [d^2 - x^2 - 2d\beta], \quad (13)$$

in flow direction ( $v_z$ ) at position  $x$ , to the simulated data via the slip length  $\beta$ . We validate this approach by comparing the measured mass flow rate  $\int \eta v(x) dx$  to the theoretical mass flow without boundary slip and find a very good agreement. The pressure gradient  $\frac{\partial P}{\partial z}$  is realized by a fixed inflow pressure ( $P(z=0) = c_s^2 \eta(z=0) = 0.3$  if not stated otherwise). At the outflow ( $z = z_{\max}$ ) we linearly extrapolate the density gradient by setting  $\eta(z_{\max}) = 2\eta(z_{\max} - 1) - \eta(z_{\max} - 2)$  in order to simulate infinite plates. Therefore, the body force regulates the velocity. The dynamic viscosity  $\mu$  as well as the pressure gradient  $\frac{\partial P}{\partial z}$  needed to fit equation (13) are obtained from our simulation data.

In a previous work (25), we have shown that this model creates a larger slip  $\beta$  with stronger interaction, namely larger  $g_{\alpha, \text{wall}}$  and larger  $\eta^{\text{wall}}$ . The relaxation time  $\tau^\alpha$  was kept constant at 1.0 in this study and the maximum available slip length measured was 5.0 in lattice units. For stronger repulsive potentials, the density gradient at the fluid-wall interface becomes too large, causing the simulation to become unstable. At lower interactions the method is very stable and the slip length  $\beta$  is independent of the distance  $d$  between the two plates and therefore independent of the resolution. We have also shown that the slip decreases with increasing pressure since the relative strength of the repulsive potential compared to the bulk pressure is weaker at high pressure. Therefore, the pressure reduction near the wall is less in the high pressure case than in the low pressure one. Furthermore, we have demonstrated that  $\beta$  can be fitted with a semi analytical model based on a two viscosity model.

## 4 Results

We have studied the dependence of the slip length  $\beta$  on the flow velocity for a wide range of velocities of more than three decades as it can be seen in Fig. 1 a) and in (25). In the figure, we show data for different fluid-wall interactions  $0 < \eta^{\text{wall}} < 2.0$  and flow velocities from  $10^{-4} < v < 10^{-1}$ . Within this region we confirm the findings of many steady state experiments (48; 49), i.e., that the slip length is independent of the flow velocity and only depends on the wettability of the channel walls. Experimentalists often present measurements for different shear rates  $S$ , which for Poiseuille flow are given by

$$S = \frac{\partial u}{\partial x}|_{x=d} = -\frac{\nabla p x}{\mu}|_{x=d} = -\frac{\nabla p d}{\mu}. \quad (14)$$

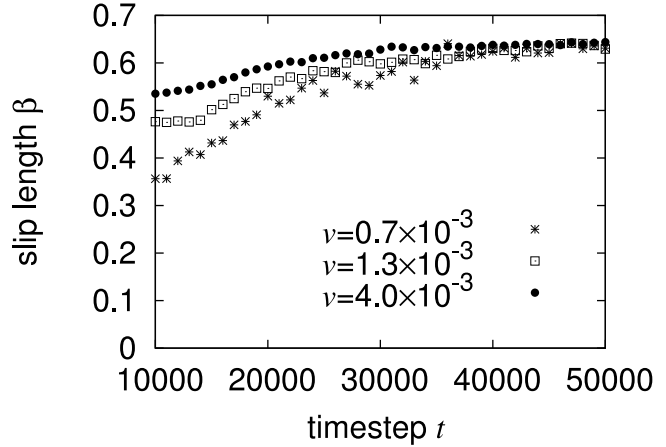
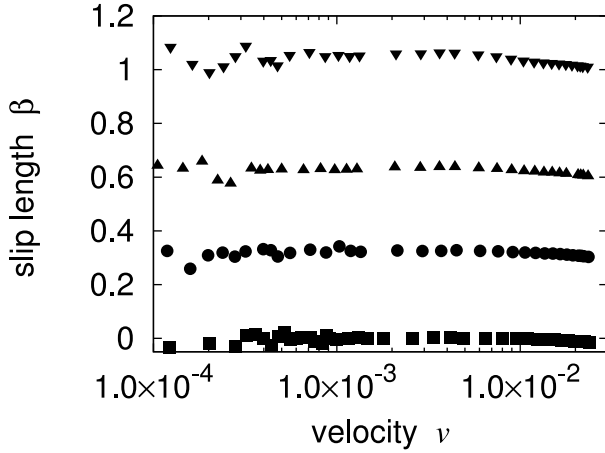


Figure 2: Measured slip length  $\beta$  versus time  $t$  for different bulk velocities at constant  $\eta^{\text{wall}} = 1.0$ . The difference between the converged slip length and the slip length during the transient is greater for slower velocities. After the convection time  $t_c = L_z/v$  the slip is converged, but already for  $t > 50000$  only small deviations from the final value can be observed.

Some dynamic experiments, however, find a shear rate dependent slip (8; 50; 51). These experiments often utilize a modified atomic force microscope as described in the introduction to detect boundary slippage. Since the slip length is found to be constant in our simulations after sufficiently long simulation times, we investigate the behavior of the slip during the transient, i.e., for simulation times  $t \ll t_c$  with  $t_c = L_z/v$  being the self convection time. The flow that is initially at rest has not converged to its final steady state. The time development of the slip length could explain an apparent shear dependence as shown in Fig. 1 b), where  $\beta$  is plotted over the flow velocity for different fluid-wall interactions at  $t = 15000$ . Here, the detected  $\beta$  depends very strongly on the flow velocity. The figure shows a qualitative similarity to the data presented in (50), namely there seems to be a critical shear rate at which the slip starts to increase very fast. However, this

a)



b)

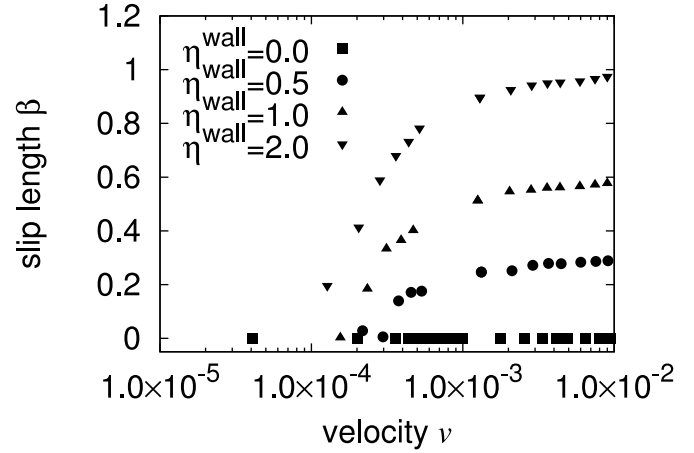


Figure 1: Slip length  $\beta$  versus bulk velocity  $v$  (on a logarithmic scale), for different fluid-wall interactions  $\eta^{\text{wall}}$  after a)  $t = 50000$  and b)  $t = 15000$  time steps. For better visibility, both figures share the same legend. The slip length is independent of the flow velocity after 50 000 timesteps and only depends on  $\eta^{\text{wall}}$  (Fig. a)). After 15000 timesteps, however, the slip length starts at a critical minimum velocity and appears to rise with increasing  $v$  (Fig. b)). Even though the mean flow velocity has reached its final value already and the parabolic velocity profile is well developed, the system is still in a transient state at  $t = 15000$  (see Fig. 3)) resulting in an eventually misleading measurement of  $\beta$ . All units are expressed in lattice units throughout this paper.

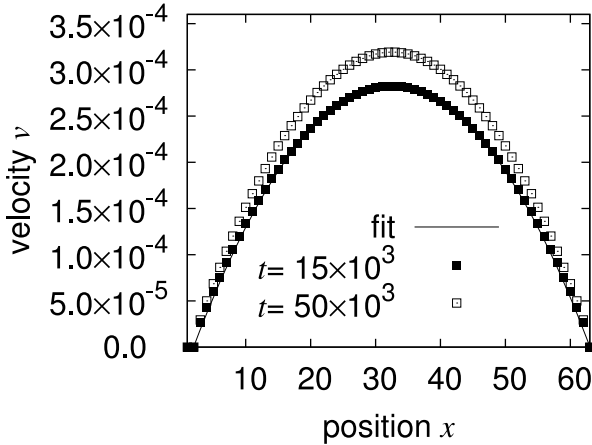


Figure 3: The velocity profile  $v(x)$  for  $\eta^{\text{wall}} = 2.0$  after  $t = 15000$  and  $t = 50000$  time steps. The lines are the parabolic fit with equation (13) with a slip length of  $\beta = 0.55 \pm 7 \cdot 10^{-3}$  at  $t = 15000$ . After 50000 time steps the slip length is significantly larger at  $\beta = 1.088 \pm 7 \cdot 10^{-4}$ .

only holds during the transient as shown in Fig. 1 – in the steady state the slip is independent of the velocity.

Fig. 2 depicts the time dependence of the measured slip length at constant  $\eta^{\text{wall}} = 1.0$  and for final flow velocities  $v = 0.7 \cdot 10^{-3}$ ,  $1.3 \cdot 10^{-3}$ , and  $4.0 \cdot 10^{-3}$ . Since for  $t < 10000$  the expected parabolic velocity profile is not developed, we only plot our data for  $10000 < t < 50000$ . It can be observed that the slip length develops to its final value for all three bulk velocities. However, the number of timesteps needed to achieve the steady state of  $\beta$  is dependent on  $v$ . The slip has reached its steady state after the convection

time  $t_c = L_z/v$ , which is the time it takes for an individual fluid element to be transported through the whole system. The slip converges with different rates depending on the flow velocity, but after 50000 timesteps the difference between the actual slip length and the converged one is neglectable already. This explains the fluctuations for very low velocities in Fig. 1a). The determination of the correct slip length therefore can only be expected after sufficiently long simulation times. As can be seen from Fig. 3, it is not sufficient to just check if the velocity profile seems to have reached its final shape. Here, velocity profiles after 15000 and 50000 timesteps are shown for a representative simulation run and  $\eta^{\text{wall}} = 2.0$ . Even though the parabolic velocity profile is already fully developed after 15000 timesteps, the measured slip length is  $\beta = 0.55 \pm 7 \cdot 10^{-3}$  only, while after 50000 timesteps  $\beta = 1.088 \pm 7 \cdot 10^{-4}$  is obtained. The solid lines in Fig. 3 correspond to a fit of the data with equation (13).

The kinematic viscosity  $\nu$  is another important parameter in fluid dynamics. However, in experiments it can only be varied by changing the fluid itself and therefore it is inevitable to change other parameters too. Within the lattice Boltzmann method with BGK collision operator (4), the kinematic viscosity of the fluid is given by (5) and depends on the relaxation time  $\tau^\alpha$ . Within the Shan-Chen model, a change of  $\tau^\alpha$  also has an influence on the effect of the body force that enters the BGK operator to model the fluid-fluid interactions. One might argue that this is not realistic since a change of viscosity does not necessarily modify the fluid-fluid interactions between different species. Additionally, it is known that mid grid bounce back boundary conditions are second order correct while using the BGK collision operator, as it is used in

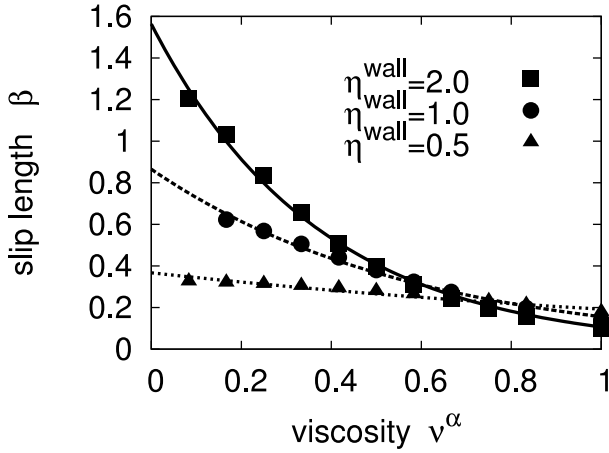


Figure 4: Corrected slip length  $\beta(\eta^{\text{wall}}) - \beta(\eta^{\text{wall}} = 0.0)$  versus kinematic viscosity  $\nu^\alpha$  for  $\eta^{\text{wall}} = 0.5, 1.0$ , and  $2.0$ . The slip length converges to 0 as shown by the solid lines representing an exponential least squares fit of the data.

this paper (23; 52). For relaxation times  $\tau^\alpha \approx 1$  the error introduced due to the boundary condition is neglectable. However, we are interested in studying the dependence of boundary slippage on the fluid's viscosity. Therefore, we performed simulations with  $\eta^{\text{wall}} = 0$ , i.e., without any fluid-wall repulsion, to estimate the effect of the error induced by the boundaries. For  $\eta^{\text{wall}} = 0$ ,  $\beta$  should be zero as well, but we find the error of the slip length being proportional to  $(\tau^\alpha)^2$ . This behavior is expected by the theory of He et al. (52) and can only be avoided by using a multi relaxation time approach. For  $1 < \tau^\alpha < 3$  the numerical error is less than 5% of the slip length while for larger relaxation times the error increases strongly so that the slip seems to increase. In order to reduce the influence of the error introduced by the single relaxation time method and the particular boundary conditions used, we subtract the slip length determined for  $\eta^{\text{wall}} = 0$  from the measured  $\beta$  at  $\eta^{\text{wall}} > 0$ . The results are plotted in Fig. 4, where we demonstrate a decreasing slip length with increasing viscosity for  $\eta^{\text{wall}} = 0.5, 1.0$ , and  $2.0$ . The data shown in Fig. 4 can be fitted exponentially as depicted by the solid lines and all three curves converge to zero for high viscosities.

Since surfactant molecules consist of a hydrophobic and a hydrophilic part, they like to assemble at the interface between a fluid and wetting or non-wetting walls. As found by experimentalists, in a wetting microchannel, this can cause no slip to switch to partial slip (49; 51). In a non-wetting environment, the surfactant molecules can shield the hydrophobic repulsion of the surface (6). We apply the amphiphilic lattice Boltzmann model as described earlier in this paper to model a fluid within a hydrophobic microchannel that contains a surfactant concentration of up to 33%. The interaction parameters are chosen according to earlier works (40; 41; 42; 43; 44; 45; 46), in such a way that they are not too strong to cause structuring effects in the flow, but strong enough to have an effect at the

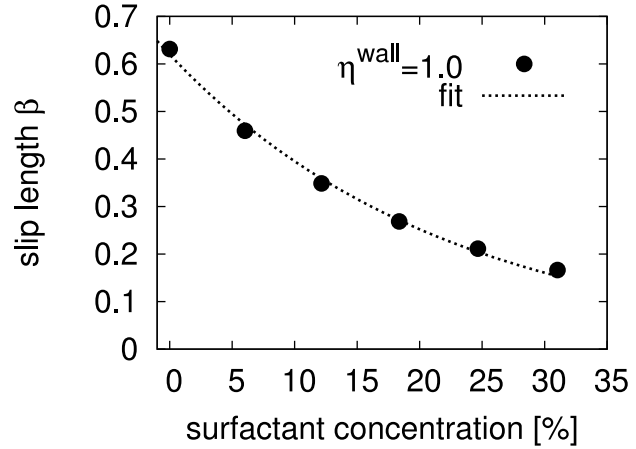


Figure 5: Slip length  $\beta$  versus the concentration of surfactant in % for  $\eta^{\text{wall}} = 1.0$ .  $\beta$  is steadily decreasing with increasing the surfactant concentration from 0.64 down to 0.19. The dashed line is given by a fit of the data with an exponential function.

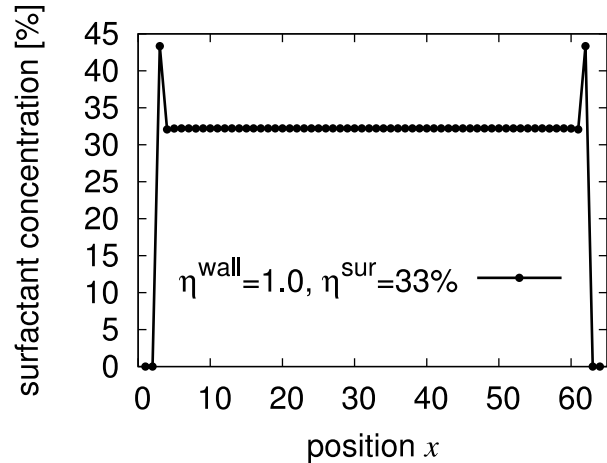


Figure 6: A typical profile of the surfactant concentration in  $x$  direction, i.e., between the channel walls. Near the surface, the surfactant concentration is substantially higher (44%) than in the bulk (32%) since it is energetically more favorable for the surfactant molecules to arrange at the fluid-surface interface, thus shielding the repulsive potential of the hydrophobic channel wall.

fluid-solid boundary. The total density inside our system  $\eta^\alpha + \eta^{\text{sur}}$  is kept fixed at 0.3. As initial condition the system is filled with a binary mixture of surfactant and fluid. The orientation  $\mathbf{d}$  of the dipoles is chosen randomly. In Fig. 5, we plot the measured slip length for fluid-wall interactions determined by  $\eta^{\text{wall}} = 0.5, 1.0$  and  $2.0$  versus the concentration of surfactant. The symbols in Fig. 5 are given by the simulation data while the lines correspond to a fit with an exponential function. We find a strong decrease of the slip length with a higher surfactant concentration. For all three values of  $\eta^{\text{wall}}$ , the measured slip lengths converge to the same value at high surfactant concentrations

showing that at high concentrations the amount of surfactant that can assemble at the interface is saturating.

In Fig. 6 we present a representative density profile of the surfactant for  $\eta^{\text{wall}} = 1.0$ . The initial amphiphile concentration is set to 33% here. It can be seen that the concentration at the first lattice site next to the surface increases to 44%, while the bulk concentration stays constant at 32% – a value slightly lower than the initial 33%. This high concentration regime close to the boundary causes the hydrophobic potential of the wall to be shielded and results in a decreasing slip. Our findings are consistent with experimental results (49; 6; 51).

Large amphiphilic molecules or polymer brushes show a shear dependent slip (53) since they have to align with the shear forces acting on them. The higher the shear force, the more they are rotated causing the effect of shielding the hydrophobicity to be reduced. Since in our model the amphiphiles are point-like, we cannot expect to observe any shear rate dependence of  $\beta$ .

---

## 5 Conclusion

---

In conclusion we have presented three-dimensional multi-phase lattice Boltzmann simulations which govern a wide range of slip phenomena. After demonstrating the validity of our model, we presented studies of the dependence of the boundary slip on the flow velocity. While the slip is independent of the velocity if the system is in the steady state, we find an apparent velocity dependence during early times of the simulation. For small numbers of timesteps, the parabolic velocity profile is already well developed, but due to the system being in a transient state, the detected slip is not correct. This is an important finding for experimental setups since to the best of our knowledge only dynamic experiments find a velocity dependence, while static experiments confirm the slip lengths being independent of the flow velocity. Our findings are in good agreement with most non dynamic experiments (1; 2) and MD simulations (18; 19).

For experimentalists it is a major effort to change the viscosity of the fluid without changing any other parameters of their setup. In computer simulations, however, this can be done easily. In our simulations we found a decrease of the detected slip with increasing viscosity.

With a simple dipole model we were able to simulate the shielding of the repulsive potential between hydrophobic walls and a fluid if surfactant is present in the solution, i.e., the slip length decreases with increasing surfactant concentration. However, we were not able to show a shear dependence as it is seen in experiments with polymer chains. In a future work, we plan to extend our simulations to govern larger molecules which can be affected by a shear flow. Then, we hope to be able to study the shear rate dependence of boundary slippage.

---

## Acknowledgements

---

We would like to thank S. Succi, L. Biferale, R. Delgado-Buscalioni, and L.S. Luo for fruitful discussions. We acknowledge the Neumann Institute for Computing for providing access to their IBM p690 system and the High Performance Computing Center Stuttgart for the possibility to use their NEC SX8. We are grateful for financial support provided by the Landesstiftung Baden-Württemberg and the DFG within priority program 1164.

---

## REFERENCES

---

- [1] E. Lauga, M. Brenner, and H. Stone. *Microfluidics: The No-Slip Boundary Condition*, in *Handbook of Experimental Fluid Dynamics*, chapter 15. Springer, 2005.
- [2] C. Neto, D. Evans, E. Bonaccorso, H. Butt, and V. Craig. Boundary slip in newtonian liquids: a review of experimental studies. *Rep. Prog. Phys.*, 68:2859, 2005.
- [3] O. Vinogradova. Drainage of a thin film confined between hydrophobic surfaces. *Langmuir*, 11:2213, 1995.
- [4] O. Vinogradova and G. Yakubov. Dynamic effects on force measurements. 2. lubrication and the atomic force microscope. *Langmuir*, 19:1227, 2003.
- [5] O. Vinogradova. Implications of hydrophobic slippage for the dynamic measurements of hydrophobic forces. *Langmuir*, 14:2827, 1998.
- [6] C. Henry, C. Neto, D. Evans, S. Biggs, and V. Craig. The effect of surfactant adsorption on liquid boundary slippage. *Physica A*, 339:60, 2004.
- [7] V. Craig, C. Neto, and D. Williams. Shear dependent boundary slip in an aqueous newtonian liquid. *Phys. Rev. Lett.*, 87:054504, 2001.
- [8] C. Neto, V. Craig, and D. Williams. Evidence of shear-dependent boundary slip in newtonian liquids. *Eur. Phys. J. E*, 12:71, 2003.
- [9] E. Bonaccorso, H.-J. Butt, and V. Craig. Surface roughness and hydrodynamic boundary slip of a newtonian fluid in a completely wetting system. *Phys. Rev. Lett.*, 90:144501, 2003.
- [10] D. Tretheway and C. Meinhart. Apparent fluid slip at hydrophobic microchannel walls. *Phys. Fluids*, 14:L9, 2002.
- [11] D. Tretheway and C. Meinhart. A generating mechanism for apparent slip in hydrophobic microchannels. *Phys. Fluids*, 15:1509, 2004.
- [12] C. Navier. Mémoire sur les lois du mouvement de fluids. *Mem. Acad. Sci. Ins. Fr.*, 6:389, 1823.

- [13] P. A. Thompson and S. Troian. A general boundary condition for liquid flow at solid surfaces. *Nature*, 389:360, 1997.
- [14] P. A. Thompson and M. O. Robbins. Shear flow near solids: Epitaxial order and flow boundary conditions. *Phys. Rev. A*, 41:6830, 1990.
- [15] J. Koplik and J. R. Banavar. No-slip condition for a mixture of two liquids. *Phys. Rev. Lett.*, 80:5125, 1998.
- [16] M. Cieplak, J. Koplik, and J. R. Banavar. Boundary conditions at a fluid-solid interface. *Phys. Rev. Lett.*, 86:803, 2001.
- [17] J. Koplik, J. R. Banavar, and J. F. Willemsen. Molecular dynamics of fluid flow at solid-surfaces. *Phys. Fluids*, 1:781, 1989.
- [18] C. Cottin-Bizone, C. Barentin, E. Charlaix, L. Boequet, and J. Barrat. Dynamics of simple liquids at heterogeneous surfaces: molecular dynamics simulations and hydrodynamic description. *Eur. Phys. J. E*, 15:427, 2004.
- [19] J. Baudry and E. Charlaix. Experimental evidence for a large slip effect at a nonwetting fluid-solid interface. *Langmuir*, 17:5232, 2001.
- [20] K. Kadau, T. Germann, and P. Lomdahl. Large scale molecular dynamics simulation of 19 billion particles. *Int. J. Mod. Phys. C*, 15:193, 2004.
- [21] A. Malevanets and R. Kapral. Mesoscopic model for solvent dynamics. *J. Chem. Phys.*, 110:8605–8613, 1999.
- [22] A. Malevanets and R. Kapral. Solute dynamics in mesoscale solvent. *J. Chem. Phys.*, 112:7260, 2000.
- [23] S. Succi. *The Lattice Boltzmann Equation for Fluid Dynamics and Beyond*. Oxford University Press, 2001.
- [24] X. Nie, G. Doolen, and S. Chen. Lattice-Boltzmann simulations of fluid flows in MEMS. *J. Stat. Phys.*, 107:279, 2002.
- [25] J. Harting, C. Kunert, and H. Herrmann. Lattice Boltzmann simulations of apparent slip in hydrophobic microchannels. *Europhys. Lett.*, 75:651, 2006.
- [26] R. Benzi, L. Biferale, M. Sbragaglia, S. Succi, and F. Toschi. Mesoscopic two-phase model for describing apparent slip in micro-channel flows. *Europhys. Lett.*, 74:651, 2006.
- [27] J. Harting, M. Harvey, J. Chin, M. Venturoli, and P. V. Coveney. Large-scale lattice Boltzmann simulations of complex fluids: advances through the advent of computational grids. *Phil. Trans. R. Soc. Lond. A*, 363:1895–1915, 2005.
- [28] R. Benzi, L. Biferale, M. Sbragaglia, S. Succi, and F. Toschi. Mesoscopic modeling of a two-phase flow in the presence of boundaries: the contact angle. *Phys. Rev. E*, 74:021509, 2006.
- [29] R. Benzi, S. Succi, and M. Vergassola. The lattice Boltzmann equation: theory and applications. *Phys. Rep.*, 222:145 – 197, 1992.
- [30] P. Bhatnagar, E. Gross, and M. Krook. Model for collision processes in gases. I. Small amplitude processes in charged and neutral one-component systems. *Phys. Rev.*, 94:511–525, 1954.
- [31] S. Chen, H. Chen, D. Martínez, and W. Matthaeus. Lattice Boltzmann model for simulation of magneto-hydrodynamics. *Phys. Rev. Lett.*, 67:3776–3779, 1991.
- [32] H. Chen, S. Chen, and W. H. Matthaeus. Recovery of the Navier-Stokes equations using a lattice-gas Boltzmann method. *Phys. Rev. A*, 45:5339–5341, 1992.
- [33] Y. Qian, D. d’Humières, and P. Lallemand. Lattice BGK models for Navier-Stokes equation. *Europhys. Lett.*, 17:479–484, 1992.
- [34] X. Shan and H. Chen. Lattice Boltzmann model for simulating flows with multiple phases and components. *Phys. Rev. E*, 47:1815, 1993.
- [35] X. Shan and H. Chen. Simulation of nonideal gases and liquid-gas phase transitions by the lattice Boltzmann equation. *Phys. Rev. E*, 49:2941, 1994.
- [36] H. Chen, B. M. Boghosian, P. Coveney, and M. Nekovee. A ternary lattice Boltzmann model for amphiphilic fluids. *Proc. R. Soc. Lond. A*, 456:2043–2047, 2000.
- [37] M. Nekovee, P. V. Coveney, H. Chen, and B. M. Boghosian. Lattice-Boltzmann model for interacting amphiphilic fluids. *Phys. Rev. E*, 62:8282, 2000.
- [38] J. Chin and P. Coveney. Lattice Boltzmann study of spinodal decomposition in two dimensions. *Phys. Rev. E*, 66:016303, 2002.
- [39] N. González-Segredo, M. Nekovee, and P. Coveney. Three-dimensional lattice-Boltzmann simulations of critical spinodal decomposition in binary immiscible fluids. *Phys. Rev. E*, 67:046304, 2003.
- [40] J. Harting, M. Venturoli, and P. Coveney. Large-scale grid-enabled lattice-Boltzmann simulations of complex fluid flow in porous media and under shear. *Phil. Trans. R. Soc. Lond. A*, 362:1703–1722, 2004.
- [41] M. Nekovee and P. Coveney. Lattice-Boltzmann simulations of self-assembly of a binary water-surfactant system into ordered bicontinuous cubic and lamellar phases. *J. Am. Chem. Soc.*, 123:12380, 2001.



- [42] M. Nekovee and P. Coveney. Lattice Boltzmann simulations of self assembly of binary amphiphilic fluids into ordered lamellar and bicontinuous cubic phases. *J. Am. Chem. Soc.*, 123:12380, 2001.
- [43] N. González-Segredo and P. Coveney. Self-assembly of the gyroid cubic mesophase: Lattice-Boltzmann simulations. *Europhys. Lett.*, 65:795, 2004.
- [44] J. Harting, M. Harvey, J. Chin, and P. V. Coveney. Detection and tracking of defects in the gyroid mesophase. *Comp. Phys. Comm.*, 165:97, 2004.
- [45] G. Giupponi, J. Harting, and P. V. Coveney. Emergence of rheological properties in lattice boltzmann simulations of gyroid mesophases. *Europhys. Lett.*, 73:533, 2006.
- [46] N. González-Segredo, J. Harting, G. Giupponi, and P. V. Coveney. Stress response and structural transitions in sheared gyroidal and lamellar amphiphilic mesophases: lattice-Boltzmann simulations. *Phys. Rev. E*, 73:031503, 2006.
- [47] J. Harting, M. Venturoli, and P. V. Coveney. Large-scale grid-enabled lattice-Boltzmann simulations of complex fluid flow in porous media and under shear. *Phil. Trans. R. Soc. Lond. A*, 362:1703, 2004.
- [48] J.-T. Cheng and N. Giordano. Fluid flow through nanometer-scale channels. *Phys. Rev. E*, 65:031206, 2002.
- [49] C. Cheikh and G. Koper. Stick-slip transition at the nanometer scale. *Phys. Rev. Lett.*, 91:156102, 2003.
- [50] Y. Zhu and S. Granick. Rate-dependent slip of newtonian liquid at smooth surfaces. *Phys. Rev. Lett.*, 87:096105, 2001.
- [51] Y. Zhu and S. Granick. No-slip boundary condition switches to partial slip when fluid contains surfactant. *Langmuir*, 18:10058, 2002.
- [52] X. He, Q. Zou, L. Luo, and M. Dembo. Analytic solutions of simple flows and analysis of non-slip boundary conditions for the lattice Boltzmann BGK model. *J. Stat. Phys.*, 87:115, 1997.
- [53] R. Fetzer, K. Jacobs, A. Münch, B. Wagner, and T. Witelski. New slip regimes and the shape of dewetting thin liquid films. *Phys. Rev. Lett.*, 95:127801, 2005.

